

Cite this: *Chem. Sci.*, 2020, 11, 4138

All publication charges for this article have been paid for by the Royal Society of Chemistry

Aromaticity and sterics control whether a cationic olefin radical is resistant to disproportionation†

Julian Messelberger,^{‡a} Annette Grünwald,^{‡a} Stephen J. Goodner,^a Florian Zeilinger,^a Piermaria Pinter,^a Matthias E. Miehlich,^a Frank W. Heinemann,^a Max M. Hansmann^{ib bc} and Dominik Munz^{id *a}

We elucidate why some electron rich-olefins such as tetrathiafulvalene (TTF) or paraquat (1,1'-dimethyl-4,4'-bipyridinylidene) form persistent radical cations, whereas others such as the dimer of *N,N'*-dimethyl benzimidazolin-2-ylidene (benzNHC) do not. Specifically, three heterodimers derived from cyclic (alkyl) (amino) carbenes (CAAC) with *N,N'*-dimethyl imidazolin-2-ylidene (NHC), *N,N'*-dimethyl imidazolidin-2-ylidene (saNHC) and *N*-methyl benzothiazolin-2-ylidene (btNHC) are reported. Whereas the olefin radical cations with the NHC and btNHC are isolable, the NHC compound with a saturated backbone (saNHC) disproportionates instead to the biscation and olefin. Furthermore, the electrochemical properties of the electron-rich olefins derived from the dimerization of the saNHC and btNHC were assessed. Based on the experiments, we propose a general computational method to model the electrochemical potentials and disproportionation equilibrium. This method, which achieves an accuracy of 0.07 V (0.06 V with calibration) in reference to the experimental values, allows for the first time to rationalize and predict the (in)stability of olefin radical cations towards disproportionation. The combined results reveal that the stability of heterodimeric olefin radical cations towards disproportionation is mostly due to aromaticity. In contrast, homodimeric radical cations are in principle isolable, if lacking steric bulk in the 2,2' positions of the heterocyclic monomers. Rigid tethers increase accordingly the stability of homodimeric radical cations, whereas the electronic effects of substituents seem much less important for the disproportionation equilibrium.

Received 6th February 2020
Accepted 28th March 2020

DOI: 10.1039/d0sc00699h

rsc.li/chemical-science

Introduction

Electron-rich olefins are an exciting class of organic redox systems with potentially three stable redox states^{1–3} and are popular reductants in organic synthesis.^{4–9} Exciting applications are in particular associated with the open-shell redox state with one unpaired electron, which allows for intriguing conductive and photochemical properties. The arguably most relevant derivative, tetrathiafulvalene (TTF **1**, Fig. 1), its saturated congener **2**,^{10,11} as well as the benzannulated derivative **3** even have been called “the brick and mortar” of organic materials. They are now commonly applied in switches, solar cells, or

organic field-effect transistors (OFETs).^{12–14} Very similar redox properties are found for olefins derived from biscationic paraquat (methyl viologen, respectively; 1,1'-dimethyl-4,4'-bipyridinylidene) **4**, the related *ortho*-derivative (1,1'-dimethyl-2,2'-bipyridinylidene) **5**, the dimethylaminopyridine (DMAP) dimer **6**,¹⁵ as well as 4,4'-bipyrylene **7**.^{16–20}

The aza-analogues of TTF, *i.e.* tetraaminoethylenes or enetetramines, originate from the formal dimerization of

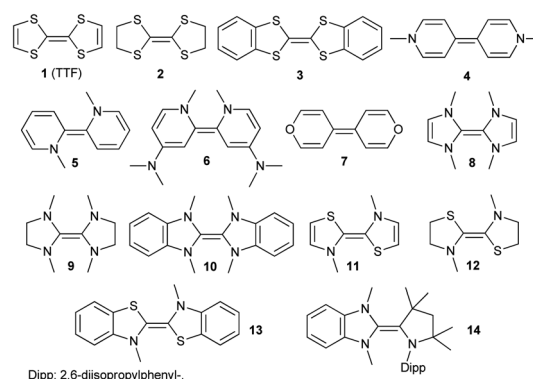


Fig. 1 Homo- (**1–13**) and heterodimeric (**14**) electron-rich olefins.

^aLehrstuhl für Allgemeine und Anorganische Chemie, Friedrich-Alexander-Universität Erlangen-Nürnberg, Egerlandstr. 1, 91058 Erlangen, Germany. E-mail: dominik.munz@fau.de

^bInstitut für Organische und Biomolekulare Chemie, Georg-August Universität Göttingen, Tammannstraße 2, 37077 Göttingen, Germany

^cOrganische Chemie, Technische Universität Dortmund, Otto-Hahn-Str. 6, 44227 Dortmund, Germany

† Electronic supplementary information (ESI) available. CCDC 1964614 and 1964615. For ESI and crystallographic data in CIF or other electronic format see DOI: 10.1039/d0sc00699h

‡ Both authors contributed equally.



unsaturated- (NHC, **8**), saturated- (saNHC, **9**) or benzannulated- (benzNHC, **10**) *N*-heterocyclic carbenes (NHCs). Other examples comprise thiazolin-2-ylidenes (**11**, **12**, **13**, Fig. 1).^{21,22} However, harnessing the exceptional electronic properties of NHC-derived electron-rich olefins for organic electronics remained challenging due to the undesired dissociation into the free carbenes (“Wanzlick’s equilibrium”).^{23–30} Whereas **8** is kinetically unstable towards dissociation,^{31–33} **10** stands in equilibrium with its monomers at room temperature.^{34,35}

Thus, we introduced electron-rich triazaolefins.³⁶ Intriguingly, heterodimer **14**, resulting from formal dimerization of a cyclic (alkyl) (amino) carbene (CAAC)³⁷ with a benzNHC, did not dissociate even upon heating to 100 °C and showed similar redox potentials as TTF (**1**: $E_{1,2} = +0.32$ V, $E_{2,3} = -0.08$ V vs. Fc/Fc⁺).¹⁴ Paralleling the rich chemistry of TTF derivatives, subsequent studies were directed at introducing bridges in order to obtain mixed-valent compounds and singlet biradicaloids.^{38–41} Other investigations explored complementary synthetic approaches^{42–45} or focused on other heterocycles as building blocks.^{46–48} In combination with further related reports,^{49–52} a considerable variety of such two-stage redox systems are now available. For applications as organic materials, it is highly desirable to predict or at least rationalize the redox potentials of these scaffolds. One of the authors suggested that the electronic properties of carbene heterodimers could be understood by the π -acceptor properties of the related free carbenes.⁴⁷ Yet, it is not understood which combinations of carbenes afford isolable radical cations upon removal of one electron. It has been proposed that the delocalization of the radical, heteroatom effects, or steric bulk might be important.¹⁷ Surprisingly and in opposition to the very stable radical cations derived from TTF, the benzNHC dimer **10** does not give a persistent radical cation. Instead, only a two-electron oxidation is observed in the cyclic voltammetry (CV) experiment with $E_{1,2} = -0.92$ V vs. Fc/Fc⁺.²¹ The electrochemical properties of **9** have not been reported according to our knowledge.

Herein, we show which factors determine whether a cationic olefin radical is stable towards disproportionation into the parent olefin and biscation. Thereby, we elucidate how electronic effects of the heteroatoms within the heterocycles, aromaticity, tethers and sterics influence the disproportionation equilibrium (Fig. 2). Based on the experimental properties of newly and previously synthesized electron-rich olefins, we propose a convenient and general concept to understand, predict and model *in silico* this disproportionation equilibrium.

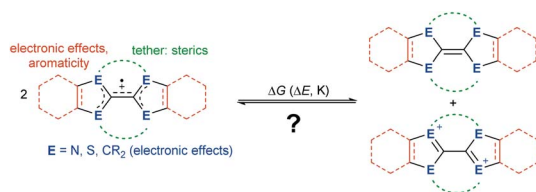


Fig. 2 What controls whether cationic olefin radicals disproportionate? ΔG , Gibbs free energy; ΔE , electrochemical potential; K , equilibrium constant.

Results and discussion

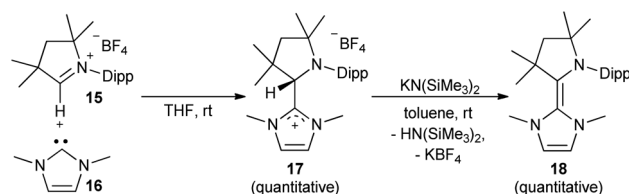
Synthesis

The synthesis of the CAAC–NHC heterodimer **18** followed the synthetic approach chosen for **14**.³⁶ The cyclic iminium salt **15** reacted swiftly at room temperature with **16** to give the colorless addition product **17** (Scheme 1). Subsequent deprotonation by potassium hexamethyldisilazide (KHMDs) afforded **18** quantitatively as a yellow solid.

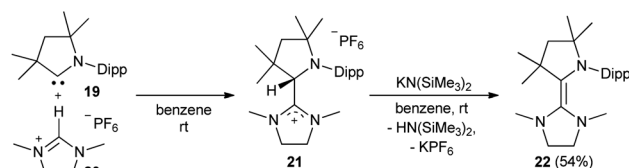
Also the addition of CAAC **19** to the imidazolium salt **20** gave **21** (Scheme 2). Subsequent deprotonation afforded the saturated heterodimer **22** after workup in 54% overall yield. These two synthetic approaches were not successful for the sulfur-containing derivative **25**, where instead the homodimer of the btNHC (**13**) formed irreversibly. However, slow addition of Hünig’s base to **15** in presence of excess of **23** led to the formation of the desired addition product **24** as a mixture with residual **15** and **13**, where the latter could be removed during the workup. Treatment with KHMDs gave then, after crystallization at -35 °C, **25** as a yellow, crystalline solid (Scheme 3).⁵³

Electrochemical properties

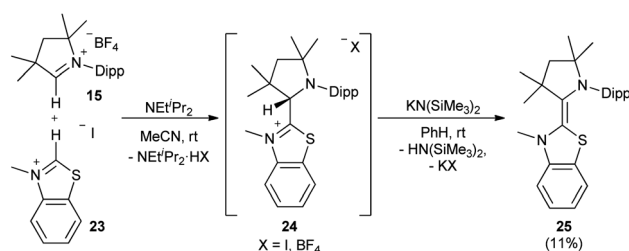
In order to elucidate the electrochemical properties of these two-stage redox-systems, CV experiments were performed (Fig. 3). All redox events were found to be reversible (Fig. S14–



Scheme 1 Formation of CAAC–NHC adduct **17** and deprotonation to **18**.



Scheme 2 Formal CH insertion of **19** and deprotonation afforded **22**.



Scheme 3 Heterodimer **25** was synthesized using Hünig’s base.



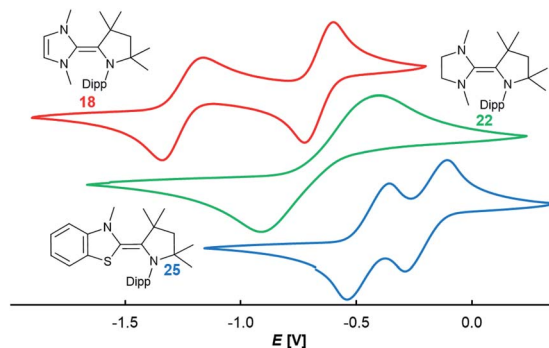


Fig. 3 CV in 0.1 M $n\text{Bu}_4\text{NPF}_6$, 100 mV s^{-1} , vs. Fc/Fc^+ in THF (18, red, $E_{1,2} = -0.67$ V, $E_{2,3} = -1.27$ V; 22, green, $E_{1,2} = -0.69$ V; 25, blue, $E_{1,2} = -0.24$ V, $E_{2,3} = -0.50$ V).

S16†). The CAAC–NHC dimer **18** showed two sequential one-electron oxidations giving rise to the stable radical cation $\mathbf{18}^{\text{rad}}$ ($E_{2,3} = -1.26$ V vs. Fc/Fc^+ in THF) and the biscation $\mathbf{18}^{\text{biscat}}$ ($E_{1,2} = -0.67$ V vs. Fc/Fc^+ in THF). Surprisingly, **22** featured only one redox wave ($E_{1,2} = -0.69$ V). The large separation of the two halfwaves of $\Delta E = 0.64$ V is indicative of a high reorganization energy and hence in this particular case of a two-electron oxidation. The btNHC derivative **25** showed two redox events ($E_{2,3} = -0.50$ V, $E_{1,2} = -0.24$ V; vs. Fc/Fc^+ in THF), which can be assigned to the oxidation of the olefin to the radical cation $\mathbf{25}^{\text{rad}}$ and the biscation $\mathbf{25}^{\text{biscat}}$, respectively. The halfwave potentials $E_{1,2}$ and $E_{2,3}$ for **25** are shifted to more positive potential in relation to the CAAC–NHC heterodimer **18**.

Comparison with the redox potentials of the CAAC–benzNHC dimer **14** ($E_{1,2} = -0.55$ V; $E_{2,3} = -0.89$ V vs. Fc/Fc^+ in THF)⁵⁴ reveals furthermore a shift to positive potential upon substitution of the methylamino group by sulfur.³⁶ However, the separation ΔE of the two redox potentials, *i.e.* the stability of the heterodimeric radical $\mathbf{25}^{\text{rad}}$ towards disproportionation, is less affected by the heteroatom substitution (**14**: $\Delta E = 0.34$ V; **25**: $\Delta E = 0.26$ V). In light of the structural analogies between the homo- (**9**, **13**) and heterodimers (**18**, **25**) derived from saNHC and btNHC, we also measured the CV for the two homodimers **9** and **13** (Fig. 4).⁵⁵ Indeed, **9** showed only a two-electron oxidation wave in dimethylformamide ($E_{1,2} = -1.26$ V vs. Fc/Fc^+),⁵⁶ while homodimer **13** featured two reversible waves separated by $\Delta E = 0.15$ V in acetonitrile.⁵⁷ Unfortunately, no CV could be obtained

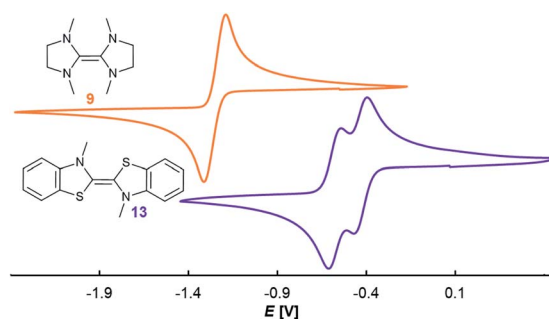
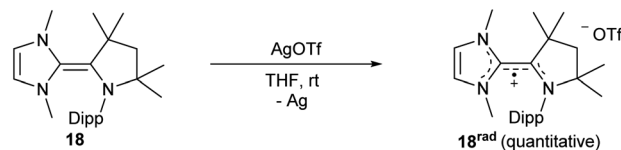


Fig. 4 CV in 0.1 M $n\text{Bu}_4\text{NPF}_6$, 100 mV s^{-1} , vs. Fc/Fc^+ (**9**, orange, $E_{1,2} = -1.27$ V in DMF; **13**, purple, $E_{1,2} = -0.45$ V, $E_{2,3} = -0.60$ V in MeCN).



Scheme 4 Synthesis of radical cation $\mathbf{18}^{\text{rad}}$ through oxidation with AgOTf .

for **9** in acetonitrile. However, a survey of reported potentials of electron-rich olefins (Table S1†) gratifyingly revealed that solvation effects on the separation of the two redox waves, subject of research herein, typically amount to less than 0.1 V.⁵⁸

Radical cation generation: oxidation of heterodimer **18**

Following the electrochemical studies, we aimed for the isolation of the radical cation $\mathbf{18}^{\text{rad}}$. Treatment of **18** with silver triflate led indeed to the quantitative formation of deeply red colored $\mathbf{18}^{\text{rad}}$ (Scheme 4).

Compound $\mathbf{18}^{\text{rad}}$ features an EPR spectrum in THF at room temperature with a g -value of 2.0019 and hyperfine coupling to three non-equivalent nitrogen atoms ($a_1 = 12.2$ MHz; $a_2 = 13.0$ MHz; $a_3 = 14.1$ MHz; Fig. 5). To further corroborate the structure of the radical cation $\mathbf{18}^{\text{rad}}$, single crystals were obtained by vapor diffusion of diethyl ether into a saturated solution in tetrahydrofuran. Single crystals of two polymorphs **A** (red) and **B** (orange) were obtained from the same batch (Fig. 6). These two polymorphs showed similar structural parameters as had been reported for $\mathbf{14}^{\text{rad}}$.³⁶ The C1–C2 bonds [**A**: 1.446(2) Å; **B**: 1.449(3) Å] are significantly longer than olefinic double bonds [**1**: 1.349(3) Å; ⁵⁹**14**: 1.346(2) Å],³⁶ but comparable in length to the C–C bond reported for $\mathbf{14}^{\text{rad}}$ [1.439(3) Å].³⁶ Strikingly however, the dihedral angle between the two carbene moieties differed considerably for the two polymorphs [N1–C1–C2–N2 for **A**: 117.2(2)°; N1–C1–C2–N2 for **B**: 50.3(3)°]. We conclude that a discussion of solid-state dihedral angles should be taken with caution.

Computations: what makes a cationic radical persistent?

Generally, “potential inversion” (*i.e.*, a seemingly two-electron redox process) is opposed to a “normal ordering” of well-behaved one-electron redox events.

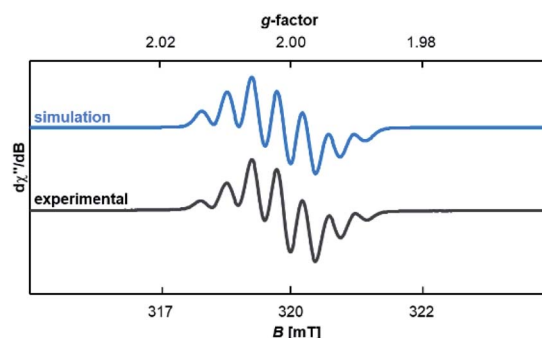


Fig. 5 Experimental and simulated EPR spectra of $\mathbf{18}^{\text{rad}}$ in THF.



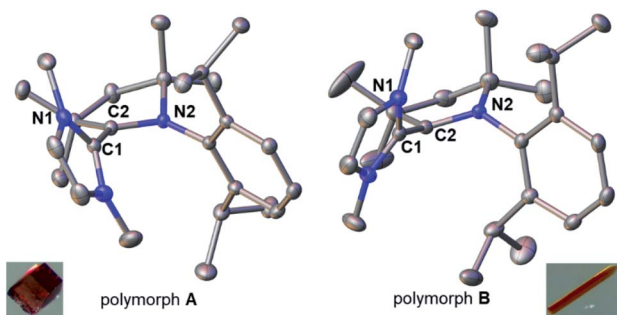


Fig. 6 Solid-state structures and colors of the two polymorphs A (left) and B (right) of the radical cation in 18^{rad} . Ellipsoids are shown at the 50% probability level; hydrogen atoms and triflate anions are omitted for clarity. Selected bond lengths [Å] and dihedral angle [°] for A: C1–C2 1.446(2), C1–N1 1.386(2), C2–N2 1.359(2); N1–C1–C2–N2 117.2(2)°. Selected bond lengths [Å] and dihedral angle [°] for B: C1–C2 1.449(3), C1–N1 1.396(2), C2–N2 1.357(2); N1–C1–C2–N2 50.3(3)°.

A two-electron transformation occurs in a two-stage redox system, if the addition of the second electron proceeds with greater ease than for the first (Scheme 5).⁶⁰ Despite continuous improvement in the recent decades,⁶¹ the solution phase thermodynamical data of chemical reactions comprising charge transfer remain often challenging to predict accurately.⁶² Indeed, we did not obtain a satisfying correlation between experiments and computations using computationally efficient implicit solvation for the two-stage redox systems studied herein (Fig. S28†). Contrarily, conceptual DFT (density functional theory),⁶³ which relies on the energy of the frontier orbitals, seems an attractive alternative. Indeed, conceptual DFT has been applied to predict electrochemical potentials of one-stage redox systems (eqn (1)).⁶⁴

$$\mu = -\chi = -\frac{1}{2}(\text{IP} + \text{EA}) \approx \frac{1}{2}(\varepsilon^{\text{HOMO}} + \varepsilon^{\text{LUMO}}) \quad (1)$$

There, the chemical potential μ of a compound corresponds to the Mulliken electronegativity χ .⁶⁵ The mean of the vertical ionization potential (IP) and electron affinity (EA), which defines the Mulliken electronegativity, can be expressed by the frontier orbital energies.^{66–68} The ionization potential is related with the eigenvalue, *i.e.* the energy of the highest occupied molecular orbital (HOMO) $\varepsilon^{\text{HOMO}}$. Correspondingly, the electron affinity is related to the energy of the singly occupied molecular orbital (SOMO) after addition of one electron (*i.e.*, the vertical electron affinity). The latter value can be sometimes approximated by the energy of the lowest unoccupied molecular orbital (LUMO) or the energy of the lowest unoccupied β -orbital in case of a radical, respectively. Pearson suggested that eqn (1) should be replaced by eqn (2) for an “oxidized” compound without significant ionization potential.⁶⁹ The value of the

chemical potential is then equivalent to the electron affinity (eqn (2)).

$$\mu = -\text{EA} \approx \varepsilon^{\text{LUMO}} \quad (2)$$

In order to model the electrochemical properties of two-stage redox systems, we propose the following method: reconsidering the redox processes depicted in Scheme 5, the chemical potential μ_1° for the biscations, which are very difficult to be further oxidized, should be solely related with their electron affinity according to eqn (2). Differently, the chemical potential μ_2° for the reduction of the cationic radicals should be approximated by eqn (1). Importantly, the cationic radicals will only be resistant towards disproportionation, if the reductive formation of the radical cation **FROM** the biscation (μ_1°) is more favorable than further reduction **TO** the olefin (μ_2°). Consequently, a persistent radical cation is formed ($\Delta\mu^\circ > 0$), if the first reduction to give the radical cation (μ_1°) is more facile than the second reduction to the olefin (μ_2°).

The difference of eqn (1) and (2) (eqn (3)–(5)) should hence describe the separation of the two redox waves $E_{1,2}$ and $E_{2,3}$ (ΔE) in experimental CVs.

$$\Delta E \propto -\Delta\mu^\circ = \mu_2^\circ - \mu_1^\circ \quad (3)$$

$$\Delta E \propto [-\text{EA}]^{\text{biscation}} + \frac{1}{2}[(\text{IP} + \text{EA})]^{\text{radical}} \quad (4)$$

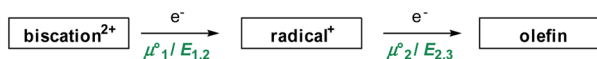
$$\Delta E \propto [\varepsilon^{\text{LUMO}}]^{\text{biscation}} - \frac{1}{2}[(\varepsilon^{\text{HOMO}} + \varepsilon^{\text{LUMO}})]^{\text{radical}} \quad (5)$$

The chemical potential $\Delta\mu$ (unit: electronvolt eV) is the molecular equivalent to the molar Gibbs free energy ΔG and both values are interconvertible using Avogadro's constant and the elementary charge of an electron (*i.e.*, Faraday's constant F). Accordingly, it is directly connected with the electrochemical potential ΔE (unit: volt V) as well as the equilibrium constant K of a reaction *via* Nernst's equation (eqn (6); RT/zF , Nernst factor; R , ideal gas constant; T , temperature; z , number of electrons; F , Faraday constant). A negative sign for $\Delta\mu$ hence indicates an exergonic reaction, *i.e.* disproportionation of the cationic radical to the olefin and biscation.

$$\Delta E = \Delta E^\circ + \frac{RT}{zF} \ln K = -\frac{\Delta G}{zF} = -\Delta\mu \quad (6)$$

We performed the quantum chemical calculations on the B3LYP-D3BJ/def2-TZVPP//B3LYP-D3BJ/def2-SVP level of theory. Thereby, we were aiming at a straightforward computational protocol of general applicability. As discussed above, solvation has sometimes an influence on the redox potentials.⁵⁶ A literature survey reveals nevertheless that it affects the electronic coupling of electron-rich olefins by less than 0.1 V (*cf.* Table S1†). Furthermore note that most electrochemical data have been reported in various solvents due to solubility, stability and resolution challenges.

Indeed, the first oxidation step $E_{1,2}$ for the homodimers was well ($R^2 = 0.94$) reproduced by calculating the chemical



Scheme 5 Stepwise reduction to give the electron-rich olefin.



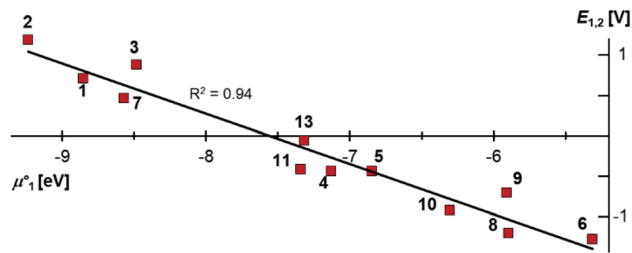


Fig. 7 The experimental halfwave potentials $E_{1,2}$ of the homodimers are linearly correlated with the calculated chemical potential μ_1° according to eqn (2). $E_{1,2}$ is given vs. SCE.

potential μ_1° using eqn (2) (Fig. 7). A worse fit was obtained when approximating the electron affinity with the respective LUMO energies (Fig. S19;† $R^2 = 0.88$). Accordingly, no satisfying correlation was obtained with eqn (1) (Fig. S20;† $R^2 = 0.60$). The second redox step $E_{2,3}$ was well ($R^2 = 0.93$) reproduced with eqn (1) (Fig. 8), where the energies of the α -HOMO and β -LUMO were used for the ionization potential and the electron affinity, respectively.⁷⁰ Modelling ΔE of the two halfwaves showed an equally good agreement with the experimental data (Fig. 9; $R^2 = 0.94$). Also here, reasonable results were only (Fig. S22–S24†) obtained when using eqn (2) for μ_1° and eqn (1) for μ_2° . Impressively, the accuracy (mean absolute deviation MAD) of the computational predictions is within 0.06 V deviation from the experiment (0.07 V if including the further examples discussed below; Table S2†). The calculations predict a large

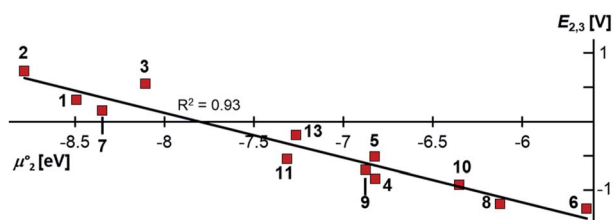


Fig. 8 The experimental halfwave potentials $E_{2,3}$ of the homodimers are linearly correlated with the calculated chemical potential μ_2° according to eqn (1). $E_{2,3}$ is given vs. SCE.

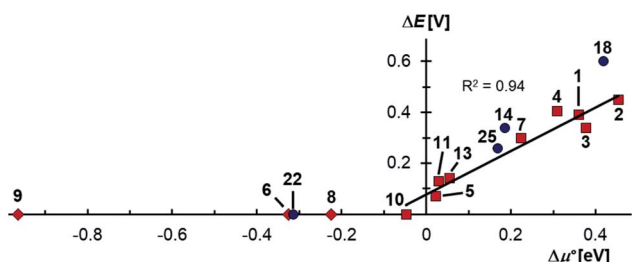


Fig. 9 The thermodynamic stability towards disproportionation of the cationic radicals (ΔE) is linearly correlated with the difference of the calculated chemical potentials in the gas phase ($\Delta\mu^{\circ} = \mu_2^{\circ} - \mu_1^{\circ}$). Heterodimers are given in blue circles, homodimers are given in red squares and diamonds. Heterodimers and homodimers given in red diamonds are not included in the linear regression.

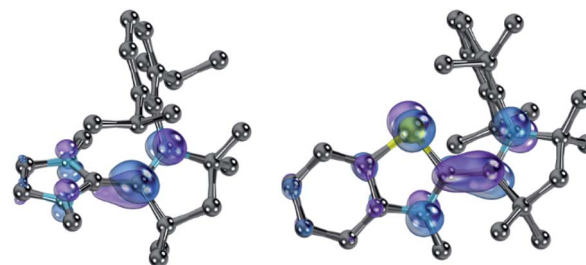


Fig. 10 SOMOs of 18^{rad} (left) and 25^{rad} (right).

separation for TTF **1** ($\Delta E = 0.4$ V; $\Delta\mu^{\circ} = 0.36$ eV) and saTTF **2** ($\Delta E = 0.5$ V; $\Delta\mu^{\circ} = 0.45$ eV) and two-electron processes for the NHC- (**8**), saNHC- (**9**) and benzNHC (**10**) homodimers ($\Delta E = 0$ V; $\Delta\mu^{\circ} < 0$). The same trend is obtained for the heterodimers **14**, **18**, **22**, **25** (Fig. S26†).

Aromaticity

Nevertheless, ΔE was both experimentally and computationally slightly larger for the hetero- than for the homodimers. We attribute this to a systematic influence of the CAAC. We found previously that the spin density in 14^{rad} is principally located on the CAAC.³⁶ The same is true for 18^{rad} and 25^{rad} (Fig. 10). This suggests that the aromaticity of the NHC moieties is more reduced in the second reduction step from the radical cations to the olefins (μ_2°) than in the first step from the biscations to the cationic radicals (μ_1°). Consequently, we had a look at the biscations' nucleus-independent chemical shift (NICS) of the NHC derived carbene rings.⁷¹ NICS is a convenient and straightforward method to approximately assess the aromaticity of planar π rings. The NICS_{0zz} value relates to the calculated out-of-plane (“zz”) part of the isotropic negative chemical NMR shift of a dummy hydrogen atom in the center of an aromatic ring. This method seems well suitable for the molecules studied herein due to the two diastereotopic faces of the aromatic rings.⁷² The more negative the chemical shift of the dummy atom, the “more aromatic” is the carbene entity.

Truly, the NICS_{0zz} values for the carbene moieties connected to the CAACs in the biscations 14^{biscat} , 18^{biscat} , 25^{biscat} as well as non-aromatic 22^{biscat} predict that increasing aromaticity (*i.e.* a more negative NICS_{0zz} value) increases the stability towards disproportionation (Fig. 11). The same order is found using experimentally determined aromaticity descriptors (Fig. S29†)^{73–76} as well as NICS scans dissecting σ -contributions (Fig. S30–S32†).^{72c} The aromaticity effect can be explained by the loss of aromatic stabilization upon reduction to the olefins. Apparently, for cationic radicals where the spin density is mainly located on the CAAC moiety, a large aromatization energy associated with the other heterocycle renders the second reduction μ_2° unfavorable and hence prevents overall the disproportionation to the olefin and biscation. For the homodimers,⁷⁷ the aromaticity seems to be almost irrelevant to the stability of the radical cations as evidenced by the large separation ΔE obtained for both aromatic **1** ($\Delta E = 0.39$ V)⁴ as well as aliphatic **2** ($\Delta E = 0.45$ V).⁷⁸ Accordingly, the aromatization energy, which originates in the



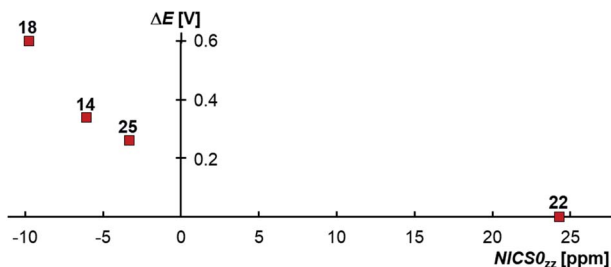


Fig. 11 CAAC-carbene heterodimeric radical cations, where the spin density is mainly located on the CAAC moiety, form isolable radical cations due to the aromaticity of the carbene heterocycles as modeled by $\text{NICS}_{0_{zz}}$. Correction for σ -effects affords a $\text{NICS}_{0_{zz}}$ value of +1.0 ppm for **22**.^{72c}

oxidation of the olefin to its biscation, does not seem to have an influence on the (in)stability of the homodimeric radical cations towards disproportionation.

Steric- and heteroatom effects

When comparing TTF (**1**) with its saturated (**2**) or benzannulated (**3**) congener, only a marginal difference was observed between the experimentally determined separation of the redox waves ΔE and the predicted chemical potentials $\Delta\mu^\circ$ ($\Delta\mu^\circ = 0.36, 0.45, 0.38$ V; Fig. 12, left). The dimers **8**, **9** and **10** are not stable towards disproportionation and the calculated redox potentials $\Delta\mu^\circ$ are consequently all negative (Fig. 12, middle). The thiazolin-2-ylidene derivatives **11**, **12**, and **13** are borderline cases (Fig. 12, right).

Although the two separate potentials $E_{1,2}, E_{2,3}$ (cf. Fig. 7 and 8) vary considerably, the stability towards disproportionation of the radical cations is also here not considerably affected. However, it is intriguing to note that all compounds with a large ΔE value (**1**, **2**, **3**, **4**, **7**) do not feature alkyl substituents in the 2,2' position of the parent carbenes. The compounds with one substituent (**5**, **11**, **12**, **13**) show moderate ΔE values, while the separation between the two halfwaves is very small for the 2,2' disubstituted heterocycles (Fig. S27[†]). For example, **1**^{rad} and **2**^{rad} with sulfur atoms in the 2,2' positions form persistent radical cations (**1**^{rad}: $\Delta E = 0.39$ V; **2**^{rad}: $\Delta E = 0.45$ V).^{4,78} Notably, the two heterocycles in these radicals are essentially coplanar (**1**^{rad}: 0° ; **2**^{rad}: 12°). Likewise, **13**^{rad} with a calculated dihedral angle of only 13° forms a stable radical cation ($\Delta E = 0.15$ V, *vide supra*).

$\Delta\mu^\circ$ [eV]	ΔE [V]	$\Delta\mu^\circ$ [eV]	ΔE [V]	$\Delta\mu^\circ$ [eV]	ΔE [V]
1 : 0.36	0.39	8 : <0	0	11 : 0.03	0.13
2 : 0.45	0.45	9 : <0	0	12 : 0.02	<i>j</i> ^a
3 : 0.38	0.33	10 : <0	0	13 : 0.06	0.14

Fig. 12 Extending the aromatic system does only have a very small influence on the stability of the homodimeric radical cations towards disproportionation (calculated: $\Delta\mu^\circ$; experimentally determined: ΔE). ^aTo the best of our knowledge, **12** has not been reported in the literature.

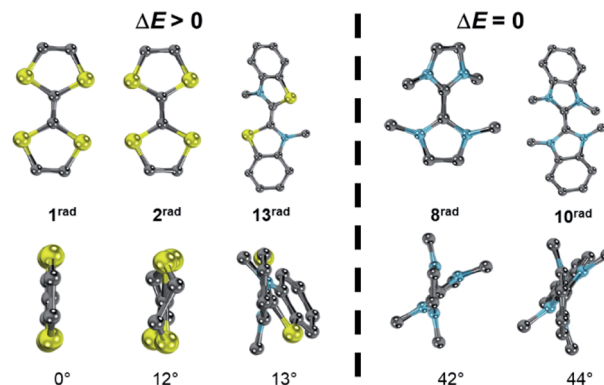


Fig. 13 Optimized structural parameters of radicals **1**^{rad}, **2**^{rad}, **8**^{rad}, **10**^{rad}, and **13**^{rad}. Side view illustrates the dihedral angle S–C–C–S' or N–C–C–N', respectively.

Contrarily, the diaminocarbene derived radical cations **8**^{rad} and **10**^{rad} with significantly larger dihedral angles of 42° and 44° disproportionate (Fig. 13). This observation can be qualitatively understood by enhanced stabilization of a delocalized radical cation, but also quantitatively using eqn (5). An enhanced twist of the radical cations leads in all cases to an increase of the ionization potential in reference to the electron affinity of the biscations. Accordingly, $\Delta\mu^\circ$ becomes negative and the radical cations disproportionate ($\Delta E = 0$ V). Contrarily, for compounds without strong structural rearrangement, the ionization potential of the radical cations is larger than the electron affinity of the biscations. This allows for an overall positive $\Delta\mu^\circ$ and hence a stable radical cation ($\Delta E > 0$ V). Following the computational predictions, we find that the steric bulk in the 2,2' position favors a twisting of the cationic radical olefins. Therefore, they disproportionate to the parent olefins and biscations.

At first sight contradicting this analysis, the replacement of the methyl substituents in **9** by phenyl groups leads to the isolable purple radical cation **Ph9**^{rad} upon one electron oxidation as evidenced by a signal in the EPR spectrum.^{79,80} In lack of detailed electrochemical data, we resynthesized Wanzlick's dimer **Ph9** and measured the CV (Fig. S11 and S12[†]).⁸¹ Notably, the CV of **Ph9** showed two overlapping, quasi-reversible redox waves with $E_{1,2} = -0.63$ V and $E_{2,3} = -0.73$ V vs. Fc/Fc^+ ($\Delta E = 0.10$ V).⁸² This is in reasonable agreement with the previously reported equilibrium constant of $K = 25$ with $K = [\text{radical-cation}]^2/([\text{olefin}][\text{biscation}])$.⁸⁰ Intriguingly, the computationally

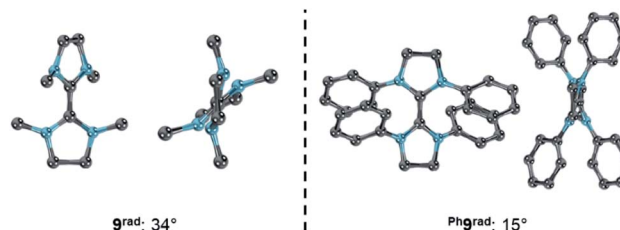


Fig. 14 Optimized structural parameters of radicals **9**^{rad} (left) and **Ph9**^{rad} (right). Side view illustrates the dihedral angle N–C–C–N'.



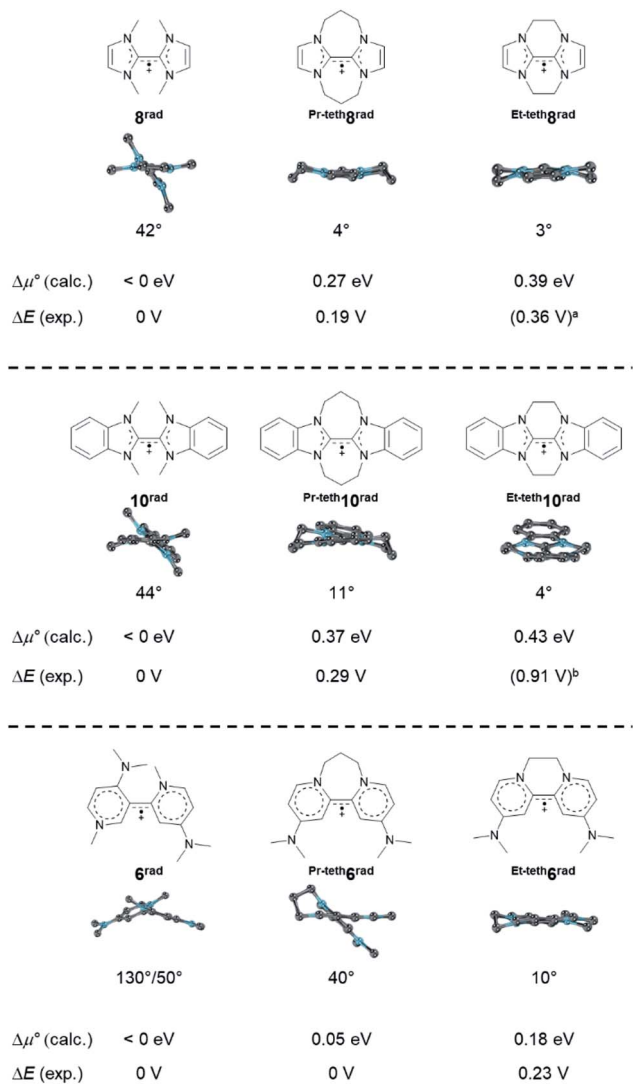


Fig. 15 Optimized structural parameters of radicals **6^{rad}**, **Et-teth6^{rad}**, **Pr-teth6^{rad}**, **8^{rad}**, **Et-teth8^{rad}**, **Pr-teth8^{rad}**, **10^{rad}**, **Et-teth10^{rad}** and **Pr-teth10^{rad}** as well as calculated and experimental CV parameters. Side view illustrates the dihedral angle N–C–C–N'. Two conformers of comparable energy ($\Delta G < 1 \text{ kcal mol}^{-1}$) were calculated for **Et-teth8^{rad}**, **Pr-teth8^{rad}**, **Et-teth10^{rad}**, and **Pr-teth10^{rad}**, given values relate to the average. ^aTo the best of our knowledge, **Et-teth8** has not been reported. Instead, the potential for mixed ethylene/propylene bridged **Et,Pr-teth8** is given. ^bHünig and coworkers question the position of $E_{2,3}$.^{84,85}

predicted difference of the chemical potentials for **Ph9** of $\Delta\mu^\circ = -0.09 \text{ eV}$ is very different to **9** ($\Delta\mu^\circ = -0.96 \text{ eV}$) and borderline in respect to forming a persistent radical cation (*cf.* Fig. 8). Examining the optimized structural parameters of the cationic radicals **9^{rad}** and **Ph9^{rad}** (Fig. 14) reveals a considerably larger dihedral angle for **9^{rad}** (34°) in reference to **Ph9^{rad}** (15°). This indicates counter-intuitively that the “bulky” phenyl groups are better accommodated in the planar than in the twisted conformation due to a coplanar orientation. Accordingly, the planar conformation of **Ph9^{rad}** is stabilized and hence prevents the disproportionation of the cationic radical. We conclude that **Ph9** is a challenging borderline case, where the computational

analysis predicts and rationalizes the surprising resistance of the cationic radical to disproportionate very well.

Inspired by the unexpected effect of the phenyl substituents on stability of the radical cation **Ph9^{rad}** towards dissociation, we eventually investigated tethers in the 2,2' positions of the homodimers (Fig. 15). We find that tethers^{33,83} increase the stability towards disproportionation. For example, whereas the disproportionation of the bisNHC radical **8^{rad}** is predicted to be exergonic ($\Delta\mu^\circ < 0 \text{ eV}$), **Pr-teth8^{rad}** ($\Delta\mu^\circ = 0.27 \text{ eV}$) and **Et-teth8^{rad}** ($\Delta\mu^\circ = 0.39 \text{ eV}$) should be persistent radicals. Indeed, this is also what had been found experimentally ($\Delta E = 0, 0.19, 0.36 \text{ V}$). The same trend was predicted for **10^{rad}** as well as the dimethylaminopyridine derivatives **6^{rad}** with only one tether. Also here, the calculated potentials are in excellent agreement with the experimental data (*e.g.*, **Et-teth6^{rad}**; $\Delta\mu^\circ = 0.18 \text{ eV}$; $\Delta E = 0.23 \text{ V}$).^{7,15} Intriguingly, the resistance of the radicals to disproportionate is also here controlled by the twist of the cationic olefin radical. Untethered and hence unperturbed **10^{rad}** shows for instance a twist of 44°, whereas the comparable long propylene linker allows for 11° and the shorter ethylene linker for only 4°. We conclude that tethers enforce a more planar, rigid structure which increases the resistance of the radical cations towards disproportionation due to enhanced resonance stabilization.

Conclusion

Although key for the design of organic electronics, it has been unclear for decades why some electron-rich olefins such as tetrathiafulvalene (TTF) or bipyridinylidenes form persistent and isolable radical cations, whereas others such as the enetetramine derived from dimerized *N,N'*-dimethyl imidazolidin-2-ylidenes (saNHC; “Wanzlick’s dimer”) do not. Herein, we showed by a combined experimental and computational investigation that sterics and aromaticity determine the stability of cationic olefin radicals towards disproportionation into the parent olefins and biscations. More specifically, we reported three electron-rich carbene heterodimers derived from a cyclic (alkyl) (amino) carbene (CAAC) in combination with saturated- (saNHC) and unsaturated *N*-heterocyclic carbenes (NHCs) as well as benzothiazolin-2-ylidene (btNHC). In order to pinpoint the differences between heterodimers and their homodimeric congeners, we also investigated the electrochemical properties of three previously reported homodimers. Importantly, the heterodimer derived from the saturated NHC does not form a persistent radical cation in opposition to the other heterodimers. We then proposed a computational method based on conceptual density functional theory to understand and predict the stability of olefin radical cations towards disproportionation. This method predicts the experimentally determined values with an accuracy of 0.07 V. We demonstrated that the persistence of CAAC-derived heterodimeric radical cations is due to aromaticity, which we suggest exploiting further in the future. Contrarily, the persistence of homodimer-derived cationic radicals is controlled almost exclusively by the steric bulk in the 2,2' positions of the parent carbenes, which we suggest deliberately harnessing as well. Neither the introduction of electron-attracting nor electron-donating groups leads to considerably increased stability towards disproportionation. Tethers however have a huge



beneficial effect, because they prevent a tilt of the carbene moieties, thus enforcing enhanced resonance stabilization of the olefin radical cation. The positive effect of sulfur atoms in the 2,2' position as present in TTF consequently is not electronic in nature. Instead, substituents in the 2,2' position sterically destabilize the cationic olefin radical through enforcement of a twisted conformation with reduced resonance stabilization.

Experimental section

All reactions were carried out under an atmosphere of dry dinitrogen, either in an MBraun dinitrogen filled glovebox or using standard Schlenk techniques. ^1H and ^{13}C NMR spectra were recorded on JEOL ECX 270, JEOL ECX 400 or Bruker Avance III HD 600 MHz instruments operating at 269.71 MHz, 399.79 MHz and 600.13 MHz for ^1H and at 67.82 MHz, 100.62 MHz and 150.90 MHz for ^{13}C , respectively and at a probe temperature of 25 °C. The solvent residual signals were used as an internal reference for the ^1H NMR and ^{13}C NMR spectra. ^1H NMR multiplicities are abbreviated as follows: s = singlet, d = doublet, dd = double of doublets, t = triplet, q = quartet, spt = septet, m = multiplet. All coupling constants J are given in Hz. Solvents were purified using a two-column solid-state purification system (Glass Contour System, Irvine, CA). Hexanes, toluene and benzene were stored over a mirror of potassium; all other solvents were stored over activated molecular sieves. Deuterated NMR solvents were obtained dry and packaged under argon and stored over activated molecular sieves or a mirror of potassium (C_6D_6). Melting points were determined using a Bibby Scientific SMP10 melting point apparatus. Elemental analyses were obtained using Euro EA 3000 (Euro Vector) and EA 1108 (Carlo-Erba) elemental analyzers. The solution EPR spectrum were recorded on a JEOL continuous wave spectrometer JESFA200 equipped with an X-band Gunn diode oscillator bridge, a cylindrical mode cavity, and a helium cryostat. The spectrum was obtained on a freshly prepared solution of 5 mM compound **18**^{rad} in THF and simulated using the eviewX and esimX programs written by E. Bill (Max-Planck-Institut für Kohlenforschung, Mülheim an der Ruhr, Germany). The EPR spectrum was measured under following conditions: microwave frequency $\nu = 8.953$ GHz, modulation width 1.0 mT, microwave power = 0.1 mW, modulation frequency = 100 kHz, time constant = 0.1 s. Electrochemical measurements were carried out at room temperature under inert atmosphere with an Autolab Type-III potentiostat. They were recorded in 0.1 M $^t\text{Bu}_4\text{NPF}_6$ solution in THF using a glassy carbon working electrode and platinum electrodes as counter and reference electrodes. Ferrocene was added as internal standard and all measurements were referenced as described in the literature. Electrochemical potentials referenced vs. the Fc/Fc^+ redox couple were converted to potentials references vs. SCE as suggested by Connelly and Geiger (Fc/Fc^+ : 0.40 V vs. SCE in MeCN; Fc/Fc^+ : 0.45 V vs. SCE in DMF; Fc/Fc^+ : 0.56 V vs. SCE in THF).⁸⁶ Electrochemical potentials referenced vs. Ag/AgNO_3 (0.01 M) and Ag/AgCl , KCl (saturated) were converted to potentials referenced vs. SCE (Ag/AgNO_3 (0.01 M): 0.30 V vs. SCE; Ag/AgCl , KCl (saturated): -0.045 V vs. SCE).^{87,88} 1,3-Dimethyl-1*H*-imidazol-3-

ium iodide, 3-methylbenzo[*d*]-thiazol-3-ium iodide **23**, the cyclic iminium salt **15** (1-(2,6-diisopropyl-phenyl)-2,2,4,4-tetramethyl-3,4-dihydro-2*H*-pyrrol-1-ium tetrafluoroborate), and free CAAC **19** were synthesized according to literature procedures.^{37a,89–92} 1,3-Dimethylimidazolium hexafluorophosphate **20** was synthesized as described in the literature⁹³ but using NH_4PF_6 instead of NH_4BF_4 . All other reagents were obtained from commercial sources and used as is without further purification. All DFT calculations were performed using ORCA 4.0.1.^{94,95} The geometry optimizations were performed at the B3LYP-D3BJ/def2-SVP level of theory^{96–99} and applying Grimme's D3 dispersion correction¹⁰⁰ with Becke–Johnson damping.^{101,102} The RIJCOSX¹⁰³ approximation in combination with the def2/J auxiliary basis set was used in order to save computation time. Tighter than default convergence criteria were chosen for both the optimization (tightopt) of the structural parameters as well as the scf iterations (tightscf) and more accurate than default grid values (Grid5, FinalGrid6) were used. All reported optimized structures were verified as true minima by the absence of negative eigenvalues in the harmonic vibrational frequency analysis. The energies of all structures were corrected by single-point calculations on the B3LYP-D3BJ/def2-TZVPP level of theory. For the calculation of μ_1^0 , the energies of the α -HOMO and the β -LUMO for the optimized structural parameters of the cationic radicals were used. For the calculation of μ_2^0 , the vertical electron affinity was used, *i.e.* the energy of the SOMO upon addition of one electron for the optimized structural parameters of the biscations.

saNHC=saNHC olefin **9**

This compound was synthesized according to a modified literature procedure. **10** was deprotonated using an equimolar amount KHMDS in benzene. Filtration and removal of volatiles afforded **9** in quantitative yield. The analytical data were consistent with the literature.¹⁰⁴

saNHC=saNHC olefin **Ph9**

This compound was synthesized according to a modified literature procedure.¹⁰⁵ *N,N'*-Diphenylethylenediamine was prepared as reported,¹⁰⁶ but purified by column chromatography (EtOAc : hexane/1 : 5, $R_f = 0.8$). The cyclization and subsequent deprotonation was performed according to the literature procedure for aryl-substituted saturated NHC olefins.¹⁰⁷ The analytical data were consistent with the values in the literature.²⁶

btNHC=btNHC olefin **13**

btNHC=btNHC olefin **13** was synthesized according to a modified literature procedure¹⁰⁸ by deprotonation of the benzothiazolium salt **23** using Hünig's base in MeCN. The ammonium salt was removed by reaction with tripotassium phosphate in Et_2O .

3-Dimethylimidazolin-2-ylidene **16**

This compound was synthesized according to a modified literature procedure.¹⁰⁹ 1,3-Dimethyl-1*H*-imidazol-3-ium iodide (2.00 g, 8.93 mmol, 1.0 eq.) and KHMDS (1.75 g,



8.75 mmol, 1.0 eq.) were combined in a Schlenk flask and suspended in Et₂O (15 mL). The mixture was stirred for 20 min at room temperature. The supernatant solution was separated from the precipitated potassium salt *via* a filter cannula. Volatiles were removed *in vacuo* to afford the carbene **16** as a pale yellow oil, which was stored at -40 °C. The low yield of only 45% (390 mg) is due to the volatility of **16** under reduced pressure. The analytical data were consistent with the values in the literature.¹⁰⁹

CAAC-NHC HBF₄ salt 17

The salt **15** (1.50 g, 4.0 mmol) and **16** (409 mg, 4.22 mmol, 1.05 eq.) were combined in a Schlenk flask and suspended in THF (20 mL). The mixture was stirred for 12 h at room temperature. The supernatant solution was removed *via* a filter cannula and the residue was washed with THF (30 mL) until the powder was colorless. The solid was dried *in vacuo* to afford **17** in quantitative yield (1.88 g). Mp.: 201 °C. ¹H NMR (600 MHz, CD₃CN) δ = 7.38 (s, 1H, NCH imidazole), 7.28 (dd, *J*₁ = 7.7 Hz, *J*₂ = 2.0 Hz, 1H, *m*-ArCH Dipp), 7.25 (t, *J* = 7.7 Hz, 1H, *p*-ArCH Dipp), 7.22 (d, *J* = 2.0 Hz, 1H, NCH imidazole), 7.12 (dd, *J*₁ = 7.3 Hz, *J*₂ = 2.0 Hz, 1H, *m*-ArCH Dipp), 5.02 (s, 1H, NCH pyrrolidine), 4.26 (s, 3H, NCH₃), 3.55 (s, 3H, NCH₃), 3.45 (spt, *J* = 6.8 Hz, 2H, 2x CH(CH₃)₂¹Pr), 2.43 (d, *J* = 13.9 Hz, 1H, CH₂ pyrrolidine), 2.29 (d, *J* = 13.9 Hz, 1H, CH₂ pyrrolidine), 1.72 (s, 3H, NCCH₃), 1.37 (d, *J* = 6.8 Hz, 3H, CHCH₃¹Pr), 1.36 (s, 3H, NCCH₃), 1.31 (d, *J* = 6.6 Hz, 3H, CHCH₃¹Pr), 1.25 (s, 3H, NCHCCH₃), 1.18 (d, *J* = 6.8 Hz, 3H, CHCH₃¹Pr), 0.96 (s, 3H, NCHCCH₃), 0.48 (d, *J* = 6.8 Hz, 3H, CHCH₃¹Pr) ppm. ¹³C NMR (101 MHz, CD₃CN) δ = 152.2 (NCN), 151.0 (ArC Dipp), 148.2 (ArC Dipp), 137.8 (ArC Dipp), 129.1 (ArCH Dipp), 127.2 (ArCH Dipp), 125.9 (ArCH Dipp), 73.4 (CCHN), 67.7 (NC(CH₃)₂), 55.2 (CH₂ pyrrolidine), 44.6 (NCC(CH₃)₂), 38.7 (NCH₃), 37.8 (NCH₃), 33.5 (CH₃ pyrrolidine), 31.7 (CH₃ pyrrolidine), 30.2 (CH₃ pyrrolidine), 28.9 (CHCH₃¹Pr), 28.4 (CHCH₃¹Pr), 27.1 (CH₃ pyrrolidine), 25.9 (CHCH₃¹Pr), 25.8 (CHCH₃¹Pr), 25.6 (CHCH₃¹Pr), 24.3 (CHCH₃¹Pr) ppm. Elemental analysis for C₂₅H₄₀F₄N₃B·0.6THF: calcd: C 64.19; H 8.81; N 8.20. Found: C 64.01; H 8.69; N 8.06%.

CAAC=NHC olefin 18

The salt **17** (1.50 g, 3.19 mmol) and KHMDS (624 mg, 3.13 mmol, 0.98 eq.) were combined in a Schlenk flask. Toluene (15 mL) was added and it was stirred for 12 h at room temperature. The supernatant solution was separated from the potassium salt *via* a filter cannula. The solvent was removed *in vacuo* and the residue was washed with hexanes. The pale yellow solid was dried *in vacuo* to afford **18** in 80% yield (970 mg). Mp.: 63 °C. ¹H NMR (270 MHz, C₆D₆) δ = 7.13–7.07 (m, 3H, ArCH Dipp), 5.71 (d, *J* = 2.1 Hz, 1H, NCH imidazoline), 5.58 (d, *J* = 2.1 Hz, 1H, NCH imidazoline), 3.55 (spt, *J* = 6.7 Hz, 2H, 2x CH(CH₃)₂¹Pr), 2.52 (s, 3H, NCH₃), 1.84 (s, 2H, CH₂ pyrrolidine), 1.69 (s, 6H, NC(CH₃)₂), 1.39 (s, 3H, NCH₃), 1.37 (d, *J* = 6.7 Hz, 6H, CH(CH₃)₂¹Pr), 1.28 (d, *J* = 6.8 Hz, 6H, CH(CH₃)₂¹Pr), 1.13 (s, 6H, NCC(CH₃)₂) ppm. ¹³C NMR (68 MHz, C₆D₆) δ = 150.1 (NCN), 143.2 (ArC Dipp), 142.7 (ArC Dipp), 129.7 (ArCH Dipp), 129.4 (ArCH Dipp), 127.4 (ArC Dipp), 126.8 (CCN), 124.9 (ArCH Dipp),

63.0 (NC(CH₃)₂), 58.4 (CH₂ pyrrolidine), 48.1 (NCH imidazoline), 44.0 (NCH imidazoline), 42.5 (NCC(CH₃)₂), 31.1 (NCH₃), 29.9 (NCH₃), 28.9 (CHCH₃¹Pr), 25.7 (CHCH₃¹Pr), 24.7 (CHCH₃¹Pr) ppm (three CH/CH₃ signals are superimposed). Elemental analysis for C₂₅H₃₉N₃: calcd: C 78.69; H 10.30; N 11.01. Found: C 78.16; H 10.35; N 10.61%.

CAAC-NHC radical 18^{rad}

Silver trifluoromethanesulfonate (AgOTf) (134 mg, 0.52 mmol, 1.0 eq.) and **18** (200 mg, 0.52 mmol, 1.0 eq.) were suspended in THF (5 mL). The mixture instantly turned deep maroon. The mixture was filtered and the solvent was removed *in vacuo* to afford **18^{rad}** as a red solid in quantitative yield (276 mg). Single crystals suitable for X-ray analysis were obtained by slow diffusion of Et₂O into a saturated THF solution at room temperature.

CAAC-NHC PF₆ salt 21

The carbene **19** (395 mg, 1.38 mmol, 1.2 eq.) and 1,3-dimethylimidazolium hexafluorophosphate (**20**) (281 mg, 1.15 mmol, 1.0 eq.) were suspended in benzene (10 mL). The mixture was stirred for 16 h at room temperature, filtered, the residue washed with benzene (2 × 2 mL) and dried *in vacuo* to give 390 mg of the crude heterodimer. This compound was used as is for the next step without further purification. ¹H NMR (270 MHz, CD₃CN): δ = 7.28–7.20 (m, 3H, ArCH Dipp), 4.77 (s, 1H, NCH pyrrolidine), 3.81–3.58 (m, 5H, CH(CH₃)₂¹Pr and H₂C-CH₂ imidazoline overlapping), 3.31 (spt, *J* = 6.5 Hz, 1H, CH(CH₃)₂¹Pr), 2.98 (s, 3H, NCH₃), 2.33 (d, *J* = 13.9 Hz, 1H, CH₂ pyrrolidine), 2.23 (d, *J* = 13.9 Hz, 1H, CH₂ pyrrolidine), 1.68 (s, 3H, NCCH₃), 1.32 (d, *J* = 6.5 Hz, 6H, CH(CH₃)₂¹Pr), 1.31 (s, 3H, NCCH₃), 1.22 (d, *J* = 6.8 Hz, 3H, CHCH₃¹Pr), 1.17 (s, 3H, NCHCCH₃), 1.16 (s, 3H, NCHCCH₃), 1.04 (d, *J* = 6.8 Hz, 3H, CHCH₃¹Pr) ppm.

CAAC=saNHC olefin 22

The salt **21** was suspended in benzene (2 mL). A solution of KHMDS (132 mg, 0.663 mmol, 0.9 eq. referring to the heterodimer salt) was added under stirring at room temperature and solids were then filtered off. Removal of volatiles afforded **22** in overall 54% yield (238 mg). Mp.: 95 °C. ¹H NMR (400 MHz, C₆D₆) δ = 7.18–7.15 (m, 1H, *m*-ArCH Dipp, superimposed by solvent), 7.12–7.11 (m, 1H, *p*-ArCH Dipp), 7.10 (d, *J* = 1.7 Hz, 1H, *m*-ArCH Dipp), 3.54 (spt, *J* = 6.8 Hz, 2H, CH(CH₃)₂¹Pr), 2.69–2.60 (m, 4H, H₂C-CH₂ imidazolidine), 2.58 (s, 3H, NCH₃), 1.89 (s, 2H, CH₂ pyrrolidine), 1.73 (s, 6H, NC(CH₃)₂), 1.63 (s, 3H, NCH₃), 1.44 (d, *J* = 6.7 Hz, 6H, CH(CH₃)₂¹Pr), 1.33 (d, *J* = 6.7 Hz, 6H, CH(CH₃)₂¹Pr), 1.19 (s, 6H, NCC(CH₃)₂) ppm. ¹³C NMR (151 MHz, C₆D₆) δ = 150.4 (NCN), 142.5 (ArC Dipp), 141.3 (ArC Dipp), 131.4 (CCN), 127.3 (ArCH Dipp), 124.5 (ArCH Dipp), 62.5 (NC(CH₃)₂), 58.0 (CH₂ pyrrolidine), 54.6 (CH₂ imidazolidine), 53.8 (CH₂ imidazolidine), 47.5 (NCH₃), 45.6 (NCH₃), 42.6 (NCC(CH₃)₂), 30.9 (CH₃ pyrrolidine), 29.7 (CH₃ pyrrolidine), 29.0 (CH(CH₃)₂¹Pr), 25.8 (CH(CH₃)₂¹Pr), 24.6 (CH(CH₃)₂¹Pr) ppm. Elemental analysis for C₂₅H₄₁N₃: calcd: C 78.27; H 10.77; N 10.95. Found: C 78.35; H 10.85; N 10.70%.



CAAC=btNHC olefin 25

The salt **15** (534 mg, 1.43 mmol, 1.0 eq.) and 3-methylbenzo[*d*]thiazol-3-ium iodide (**23**) (594 mg, 2.15 mmol, 1.5 eq.) were suspended in MeCN. Diisopropylethylamine (278 mg, 2.15 mmol, 1.5 eq.) was added dropwise over the course of 20 min at room temperature. The red suspension was stirred for 8 h and the volatiles were removed *in vacuo*. Dry K₃PO₄ (3.04 g, 14.3 mmol, 10 eq.) and Et₂O (20 mL) were added. The mixture was stirred for 24 h and filtered. The yellow solid was washed with Et₂O (3 × 5 mL) and extracted with MeCN (4 × 5 mL). The solvent was evaporated. The yellow solid was suspended in benzene (10 mL), stirred for 10 min, filtered and dried (3 ×). A solution of KHMDS (285 mg, 1.43 mmol, 1.0 eq.) in benzene (2 mL) was then added to a suspension of the yellow solid in benzene (5 mL) at room temperature. The mixture was stirred for 1 h and the volatiles were removed *in vacuo*. The heterodimer was extracted with hexanes (3 × 3 mL). The solution was concentrated to 2 mL, filtered, and cooled to –35 °C upon which crystals formed. The mother liquor was decanted after 16 h and the yellow crystals were washed with cold hexanes (2 × 1 mL). Drying *in vacuo* afforded **25** in 11% yield (67 mg). Mp.: 190–191 °C. ¹H NMR (400 MHz, C₆D₆) δ = 7.25 (dd, *J*₁ = 8.3 Hz, *J*₂ = 6.9 Hz, 1H, *p*-ArCH Dipp), 7.16–7.14 (m, 2H, *m*-ArCH Dipp, superimposed by solvent), 6.88 (dd, *J*₁ = 9.3 Hz, *J*₂ = 7.7 Hz, 2H, ArCH benzothiazoline), 6.79 (dd, *J*₁ = 8.8 Hz, *J*₂ = 7.4 Hz, 1H, ArCH benzothiazoline), 6.66 (dd, *J*₁ = 8.8 Hz, *J*₂ = 7.4 Hz, 1H, ArCH benzothiazoline), 3.40 (spt, *J* = 6.9 Hz, 2H, 2x CH(CH₃)₂ⁱPr), 2.73 (s, 3H, NCH₃), 1.78 (s, 2H, CH₂ pyrrolidine), 1.64 (s, 6H, NC(CH₃)₂), 1.47 (d, *J* = 6.9 Hz, 6H, CH(CH₃)₂ⁱPr), 1.26 (d, *J* = 6.9 Hz, 6H, CH(CH₃)₂ⁱPr), 1.13 (s, 6H, NCC(CH₃)₂) ppm. ¹³C NMR (101 MHz, C₆D₆) δ = 152.5 (NCS), 150.3 (ArCS), 148.6 (ArCN benzothiazoline), 138.2 (ArC Dipp), 137.3 (ArC Dipp), 128.4 (ArCH, superimposed by solvent), 125.1 (ArCH), 124.8 (ArCH), 124.7 (ArCH), 121.2 (ArCH), 117.4 (ArCH), 114.5 (CCN), 64.1 (NC(CH₃)₂), 58.1 (CH₂ pyrrolidine), 49.1 (NCH₃), 43.8 (NCC(CH₃)₂), 31.3 (CH₃ pyrrolidine), 30.0 (CH₃ pyrrolidine), 29.0 (CH(CH₃)₂ⁱPr), 26.0 (CH(CH₃)₂ⁱPr), 25.2 (CH(CH₃)₂ⁱPr) ppm. Elemental analysis for C₂₈H₃₈N₂S·0.05KI: calcd: C 76.26; H 8.68; N 6.35, S 7.26. Found: C 76.22; H 8.37; N 6.25, S 6.84%.

Conflicts of interest

There are no conflicts to declare.

Acknowledgements

D. M. and M. M. H. thank the Fonds der Chemischen Industrie for Liebig fellowships. Financial Support by the Boehringer-Ingelheim Fonds and the German-American Fulbright commission are gratefully acknowledged. We thank the RRZE Erlangen for computational resources. Continuous support by K. Meyer and M. Alcarazo is gratefully acknowledged.

Notes and references

- 1 R. W. Hoffmann, *Angew. Chem., Int. Ed.*, 1968, **7**, 754.

- 2 J. Hocker and R. Merten, *Angew. Chem., Int. Ed.*, 1972, **11**, 964.
- 3 M. F. Lappert, *J. Organomet. Chem.*, 1988, **358**, 185.
- 4 J. Broggi, T. Terme and P. Vanelle, *Angew. Chem., Int. Ed.*, 2014, **53**, 384.
- 5 J. A. Murphy, *J. Org. Chem.*, 2014, **79**, 3731.
- 6 E. Doni and J. A. Murphy, *Chem. Commun.*, 2014, **50**, 6073.
- 7 J. A. Murphy, J. Garnier, S. R. Park, F. Schoenebeck, S. Z. Zhou and A. T. Turner, *Org. Lett.*, 2008, **10**, 1227.
- 8 S. Z. Zhou, G. M. Anderson, B. Mondal, E. Doni, V. Ironmonger, M. Kranz, T. Tuttle and J. A. Murphy, *Chem. Sci.*, 2014, **5**, 476.
- 9 S. Rohrbach, R. S. Shah, T. Tuttle and J. A. Murphy, *Angew. Chem., Int. Ed.*, 2019, **58**, 11454.
- 10 F. Wudl, D. Wobschall and E. J. Hufnagel, *J. Am. Chem. Soc.*, 1972, **94**, 670.
- 11 S. Hünig, G. Kießlich, H. Quast and D. Scheutzow, *Liebigs Ann.*, 1973, 310.
- 12 N. Martin, *Chem. Commun.*, 2013, **49**, 7025.
- 13 D. Canevet, M. Salle, G. Zhang, D. Zhang and D. Zhu, *Chem. Commun.*, 2009, 2245.
- 14 M. Bendikov, F. Wudl and D. F. Perepichka, *Chem. Rev.*, 2004, **104**, 4891.
- 15 J. Garnier, A. R. Kennedy, L. E. A. Berlouis, A. T. Turner and J. A. Murphy, *Beilstein J. Org. Chem.*, 2010, **6**, 73.
- 16 S. Hünig, J. Groß and W. Schenk, *Liebigs Ann.*, 1973, 324.
- 17 E. Weitz, *Angew. Chem.*, 1954, **66**, 658.
- 18 S. Hünig, B. J. Garner, G. Ruider and W. Schenk, *Liebigs Ann.*, 1973, 1036.
- 19 R. J. Mortimer, *Chem. Soc. Rev.*, 1997, **26**, 147.
- 20 C. G. Claessens and J. F. Stoddart, *J. Phys. Org. Chem.*, 1997, **10**, 254.
- 21 S. Hünig, H. Schlaf, G. Kießlich and D. Scheutzow, *Tetrahedron Lett.*, 1969, **10**, 2271.
- 22 For concise and recent reviews on carbene ligands, see: (a) M. N. Hopkinson, C. Richter, M. Schedler and F. Glorius, *Nature*, 2014, **510**, 485; (b) R. S. Ghadwal, *Dalton Trans.*, 2016, **45**, 16081; (c) D. Munz, *Organometallics*, 2018, **37**, 275. For thematic issues and books on NHCs, see: (d) A. J. Arduengo and G. Bertrand, *Chem. Rev.*, 2009, **109**, 3209; (e) S. Díez González, *N-Heterocyclic Carbenes: From Laboratory Curiosities to Efficient Synthetic Tools*, Royal Society of Chemistry, Cambridge, UK, 2010; (f) T. Rovis and S. P. Nolan, *Synlett*, 2013, **24**, 1188; (g) S. P. Nolan, *N-Heterocyclic Carbenes: Effective Tools for Organometallic Synthesis*; Wiley-VCH, Weinheim, Germany, 2014; (h) H. V. Huynh, *The Organometallic Chemistry of N-heterocyclic Carbenes*, John Wiley & Sons, 2017; (i) F. E. Hahn, *Chem. Rev.*, 2018, **118**, 9455; For a review with a focus on cyclic singlet carbenes, see: (j) M. Melaimi, M. Soleilhavoup and G. Bertrand, *Angew. Chem., Int. Ed.*, 2010, **49**, 8810. For a visual tutorial on isolating free carbenes and heterodimers, see: (k) A. Grünwald, S. J. Goodner and D. Munz, *J. Visualized Exp.*, 2019, e9389.
- 23 H. W. Wanzlick and E. Schikora, *Chem. Ber./Recl.*, 1961, **94**, 2389.



- 24 H. W. Wanzlick and E. Schikora, *Angew. Chem., Int. Ed.*, 1960, **72**, 494.
- 25 Y. Liu and D. M. Lemal, *Tetrahedron Lett.*, 2000, **41**, 599.
- 26 M. K. Denk, K. Hatano and M. Ma, *Tetrahedron Lett.*, 1999, **40**, 2057.
- 27 D. M. Lemal, R. A. Lovald and K. I. Kawano, *J. Am. Chem. Soc.*, 1964, **86**, 2518.
- 28 R. W. Alder, L. Chaker and F. P. V. Paolini, *Chem. Commun.*, 2004, 2172.
- 29 R. W. Alder, M. E. Blake, L. Chaker, J. N. Harvey, F. Paolini and J. Schütz, *Angew. Chem., Int. Ed.*, 2004, **43**, 5896.
- 30 V. P. W. Böhm and W. A. Herrmann, *Angew. Chem., Int. Ed.*, 2000, **39**, 4036.
- 31 V. Gierz, J. Melomedov, C. Förster, C. Deißler, F. Rominger, D. Kunz and K. Heinze, *Chem.–Eur. J.*, 2012, **18**, 10677.
- 32 P. I. Jolly, S. Zhou, D. W. Thomson, J. Garnier, J. A. Parkinson, T. Tuttle and J. A. Murphy, *Chem. Sci.*, 2012, **3**, 1675.
- 33 T. A. Taton and P. Chen, *Angew. Chem., Int. Ed.*, 1996, **35**, 1011.
- 34 Y. Liu, P. E. Lindner and D. M. Lemal, *J. Am. Chem. Soc.*, 1999, **121**, 10626.
- 35 F. E. Hahn, L. Wittenbecher, D. Le Van and R. Fröhlich, *Angew. Chem., Int. Ed.*, 2000, **39**, 541.
- 36 D. Munz, J. Chu, M. Melaimi and G. Bertrand, *Angew. Chem., Int. Ed.*, 2016, **55**, 12886.
- 37 For the first report of a CAAC, see: (a) V. Lavallo, Y. Canac, C. Prasang, B. Donnadiou and G. Bertrand, *Angew. Chem., Int. Ed.*, 2005, **44**, 5705. For reviews on CAACs, see: (b) M. Soleilhavoup and G. Bertrand, *Acc. Chem. Res.*, 2015, **48**, 256; (c) S. Roy, K. C. Mondal and H. W. Roesky, *Acc. Chem. Res.*, 2016, **49**, 357; (d) M. Melaimi, R. Jazzar, M. Soleilhavoup and G. Bertrand, *Angew. Chem., Int. Ed.*, 2017, **56**, 10046; (e) U. S. D. Paul and U. Radius, *Eur. J. Inorg. Chem.*, 2017, 3362; For the synthesis of donor substituted CAACs, see: (f) J. Chu, D. Munz, R. Jazzar, M. Melaimi and G. Bertrand, *J. Am. Chem. Soc.*, 2016, **138**, 7884.
- 38 J. Messelberger, A. Grünwald, P. Pinter, M. M. Hansmann and D. Munz, *Chem. Sci.*, 2018, **9**, 6107.
- 39 T. Ullrich, P. Pinter, J. Messelberger, P. Haines, R. Kaur, M. M. Hansmann, D. Munz and D. M. Guldi, *Angew. Chem., Int. Ed.*, 2020, DOI: 10.1002/anie.202001286.
- 40 M. M. Hansmann, M. Melaimi and G. Bertrand, *J. Am. Chem. Soc.*, 2018, **140**, 2206.
- 41 M. M. Hansmann, M. Melaimi, D. Munz and G. Bertrand, *J. Am. Chem. Soc.*, 2018, **140**, 2546.
- 42 D. Mandal, S. Sobottka, R. Dolai, A. Maiti, D. Dhara, P. Kalita, R. S. Narayanan, V. Chandrasekhar, B. Sarkar and A. Jana, *Chem. Sci.*, 2019, **10**, 4077.
- 43 D. Mandal, R. Dolai, N. Chrysochos, P. Kalita, R. Kumar, D. Dhara, A. Maiti, R. S. Narayanan, G. Rajaraman, C. Schulzke, V. Chandrasekhar and A. Jana, *Org. Lett.*, 2017, **19**, 5605.
- 44 G. P. McGlacken and T. A. Khan, *Angew. Chem., Int. Ed.*, 2008, **47**, 1819.
- 45 A. J. Arduengo, F. Davidson, H. V. R. Dias, J. R. Goerlich, D. Khasnis, W. J. Marshall and T. K. Prakasha, *J. Am. Chem. Soc.*, 1997, **119**, 12742.
- 46 P. W. Antoni, T. Bruckhoff and M. M. Hansmann, *J. Am. Chem. Soc.*, 2019, **141**, 9701.
- 47 P. W. Antoni and M. M. Hansmann, *J. Am. Chem. Soc.*, 2018, **140**, 14823.
- 48 S. S. Hanson, E. Doni, K. T. Traboulsee, G. Coulthard, J. A. Murphy and C. A. Dyker, *Angew. Chem., Int. Ed.*, 2015, **54**, 11236.
- 49 S. V. Klementyeva, P. A. Abramov, N. V. Somov, Y. B. Dudkina, Y. H. Budnikova and A. I. Poddel'sky, *Org. Lett.*, 2019, **21**, 946.
- 50 C. M. Weinstein, C. D. Martin, L. Liu and G. Bertrand, *Angew. Chem., Int. Ed.*, 2014, **126**, 6550.
- 51 L. Y. M. Eymann, P. Varava, A. M. Shved, B. F. E. Curchod, Y. Liu, O. M. Planes, A. Sienkiewicz, R. Scopelliti, F. Fadaei Tirani and K. Severin, *J. Am. Chem. Soc.*, 2019, **141**, 17112.
- 52 B. Eberle, E. Kaifer and H. J. Himmel, *Angew. Chem., Int. Ed.*, 2017, **56**, 3360.
- 53 The Z configuration was assigned based on calculations (B3LYP/def2-SVP: $\Delta G = 4.0 \text{ kcal mol}^{-1}$) and 2D-NMR (NOESY/ROESY) spectra (Fig. S10†).
- 54 Reinvestigation of the CV data of **14** revealed that the two halfwave potentials are located at $E_{1,2} = +0.01 \text{ V}$ and $E_{2,3} = -0.33 \text{ V}$ vs. SCE.
- 55 Electrochemical data for **13** has been reported ($E_{1,2} = -0.02 \text{ V}$; $E_{2,3} = -0.17 \text{ V}$), but was repeated in order to reference vs. Fc/Fc^+ . S. Hünig, H. Schlaf, G. Kießlich and D. Scheutzow, *Tetrahedron Lett.*, 1969, **10**, 2271.
- 56 CVs in THF showed an irreversible redox wave.
- 57 CVs in THF showed a very broad wave and did not resolve the two redox events well.
- 58 For a detailed investigation of solvation effects, see: B. Eberle, O. Hubner, A. Ziesak, E. Kaifer and H. J. Himmel, *Chem.–Eur. J.*, 2015, **21**, 8578.
- 59 W. F. Cooper, N. C. Kenny, J. W. Edmonds, A. Nagel, F. Wudl and P. Coppens, *Chem. Commun.*, 1971, 889.
- 60 D. H. Evans, *Chem. Rev.*, 2008, **108**, 2113.
- 61 For leading references on the calculation of solvation free energies with a focus on electrochemistry, see: (a) A. V. Marenich, J. M. Ho, M. L. Coote, C. J. Cramer and D. G. Truhlar, *Phys. Chem. Chem. Phys.*, 2014, **16**, 15068; (b) J. M. Ho, *Phys. Chem. Chem. Phys.*, 2015, **17**, 2859; (c) J. Cheng, X. D. Liu, J. VandeVondele, M. Sulpizi and M. Sprik, *Acc. Chem. Res.*, 2014, **47**, 3522. For general references on modeling solvation effects, see: (d) V. Barone and M. Cossi, *J. Phys. Chem. A*, 1998, **102**, 1995; (e) A. V. Marenich, C. J. Cramer and D. G. Truhlar, *J. Phys. Chem. B*, 2009, **113**, 6378; (f) A. Klamt, *Wiley Interdiscip. Rev.: Comput. Mol. Sci.*, 2018, **8**, e1338; (g) W. L. Jorgensen and J. Tirado-Rives, *Proc. Natl. Acad. Sci. U. S. A.*, 2005, **102**, 6665; (h) J. Zhang, H. Y. Zhang, T. Wu, Q. Wang and D. van der Spoel, *J. Chem. Theory Comput.*, 2017, **13**, 1034.
- 62 S. Grimme and P. R. Schreiner, *Angew. Chem., Int. Ed.*, 2018, **57**, 4170.



- 63 P. Geerlings, F. De Proft and W. Langenaeker, *Chem. Rev.*, 2003, **103**, 1793.
- 64 J. Moens, P. Jaque, F. De Proft and P. Geerlings, *J. Phys. Chem. A*, 2008, **112**, 6023.
- 65 R. G. Parr and W. Yang, *Density-Functional Theory of Atoms and Molecules*, Oxford University Press, USA, 1989.
- 66 R. G. Pearson, *J. Chem. Sci.*, 2005, **117**, 369.
- 67 T. Koopmans, *Physica*, 1934, **1**, 104.
- 68 J. F. Janak, *Phys. Rev. B: Solid State*, 1978, **18**, 7165.
- 69 R. G. Pearson, *J. Mol. Struct.*, 1992, **255**, 261.
- 70 Even though μ_2^+ is seemingly also well in agreement with the experimental values for $E_{2,3}$ when using eqn 2 (Fig. S22,† $R^2 = 0.95$), a substantially worse fit (Fig. S23,† $R^2 = 0.61$) is obtained for the difference of the halfwave potentials ΔE .
- 71 (a) P. v. R. Schleyer, C. Maerker, A. Dransfeld, H. Jiao and N. J. R. van Eikema Hommes, *J. Am. Chem. Soc.*, 1996, **118**, 6317; (b) Z. F. Chen, C. S. Wannere, C. Corminboeuf, R. Puchta and P. V. Schleyer, *Chem. Rev.*, 2005, **105**, 3842; (c) R. Gershoni-Poranne and A. Stanger, *Chem. Soc. Rev.*, 2015, **44**, 6597; (d) A. Stanger, *Eur. J. Org. Chem.*, 2020, DOI: , DOI: 10.1002/ejoc.201901829.
- 72 Note that NICS values, especially NICS0, include σ -effects and hence can lead to erroneous results. (a) C. Corminboeuf, T. Heine, G. Seifert, P. V. Schleyer and J. Weber, *Phys. Chem. Chem. Phys.*, 2004, **6**, 273; (b) H. Fallah-Bagher-Shaidaei, C. S. Wannere, C. Corminboeuf, R. Puchta and P. V. Schleyer, *Org. Lett.*, 2006, **8**, 863; (c) A. Stanger, *J. Org. Chem.*, 2010, **75**, 2281; (d) A. Stanger, *J. Phys. Chem. A*, 2019, **123**, 3922.
- 73 A. T. Balaban, D. C. Oniciu and A. R. Katritzky, *Chem. Rev.*, 2004, **104**, 2777.
- 74 A. R. Katritzky, V. Feygelman, G. Musumarra, P. Barczynski and M. Szafran, *J. Prakt. Chem.*, 1990, 332.
- 75 K. E. Horner and P. B. Karadakov, *J. Org. Chem.*, 2015, **80**, 7150.
- 76 T. M. Krygowski, M. K. Cyranski and M. A. R. Matos, *Aromaticity in Heterocyclic Compounds*, Springer, Berlin, Germany, 2009.
- 77 Equally note that antiaromaticity should be important for pyrenes and pyridylidenes.
- 78 V. Khodorkovsky, A. Edzifna and O. Neilands, *J. Mol. Electron.*, 1989, **5**, 33.
- 79 D. M. Lemal and K. I. Kawano, *J. Am. Chem. Soc.*, 1962, **84**, 1761.
- 80 R. C. Wheland, *J. Am. Chem. Soc.*, 1976, **98**, 3926.
- 81 P. B. Hitchcock, *Dalton Trans.*, 1979, 1314.
- 82 CVs in THF, dimethylformamide or acetonitrile showed either a very broad wave and did not resolve the two redox events (THF, DMF) well or showed an irreversible redox wave (MeCN).
- 83 J. A. Murphy, S. Z. Zhou, D. W. Thomson, F. Schoenebeck, M. Mahesh, S. R. Park, T. Tuttle and L. E. Berlouis, *Angew. Chem., Int. Ed.*, 2007, **46**, 5178.
- 84 J. R. Ames, M. A. Houghtaling, D. L. Terrian and T. P. Mitchell, *Can. J. Chem.*, 1997, **75**, 28.
- 85 S. Hünig, D. Scheutzow, H. Schlaf and H. Pütter, *Liebigs Ann.*, 1974, 1436.
- 86 N. G. Connelly and W. E. Geiger, *Chem. Rev.*, 1996, **96**, 877.
- 87 A. J. Bard and L. R. Faulkner, *Electrochemical Methods: Fundamentals and Applications*, Wiley, New York, US, 2000.
- 88 V. V. Pavlishchuk and A. W. Addison, *Inorg. Chim. Acta*, 2000, **298**, 97.
- 89 Y. Gothe, T. Marzo, L. Messori and N. Metzler-Nolte, *Chem.–Eur. J.*, 2016, **22**, 12487.
- 90 R. Jazzar, R. D. Dewhurst, J.-B. Bourg, B. Donnadieu, Y. Canac and G. Bertrand, *Angew. Chem., Int. Ed.*, 2007, **46**, 2899.
- 91 P. Bissinger, H. Braunschweig, A. Damme, I. Krummenacher, A. K. Phukan, K. Radacki and S. Sugawara, *Angew. Chem., Int. Ed.*, 2014, **53**, 7360.
- 92 M. G. Capdevila, E. Emer, A. Gualandi, D. Petruzzello, S. Grilli and P. G. Cozzi, *ChemCatChem*, 2012, **4**, 968.
- 93 F. Hanasaka, K. Fujita and R. Yamaguchi, *Organometallics*, 2005, **24**, 3422.
- 94 F. Neese, *Wiley Interdiscip. Rev.: Comput. Mol. Sci.*, 2018, **8**, e1327.
- 95 F. Neese, *Wiley Interdiscip. Rev.: Comput. Mol. Sci.*, 2012, **2**, 73.
- 96 A. D. Becke, *J. Chem. Phys.*, 1993, **98**, 5648.
- 97 C. T. Lee, W. T. Yang and R. G. Parr, *Phys. Rev. B: Condens. Matter Mater. Phys.*, 1988, **37**, 785.
- 98 P. J. Stephens, F. J. Devlin, C. F. Chabalowski and M. J. Frisch, *J. Phys. Chem.*, 1994, **98**, 11623.
- 99 F. Weigend and R. Ahlrichs, *Phys. Chem. Chem. Phys.*, 2005, **7**, 3297.
- 100 S. Grimme, J. Antony, S. Ehrlich and H. Krieg, *J. Chem. Phys.*, 2010, **132**, 154104.
- 101 S. Grimme, S. Ehrlich and L. Goerigk, *J. Comput. Chem.*, 2011, **32**, 1456.
- 102 F. Weigend, *Phys. Chem. Chem. Phys.*, 2006, **8**, 1057.
- 103 F. Neese, F. Wennmohs, A. Hansen and U. Becker, *Chem. Phys.*, 2009, **356**, 98.
- 104 M. K. Denk, A. Thadani, K. Hatano and A. J. Lough, *Angew. Chem., Int. Ed.*, 1997, **36**, 2607.
- 105 H. W. Wanzlick, *Org. Synth.*, 1967, **47**, 14.
- 106 A. J. Arduengo, R. Krafczyk, R. Schmutzler, H. A. Craig, J. R. Goerlich, W. J. Marshall and M. Unverzagt, *Tetrahedron*, 1999, **55**, 14523.
- 107 J. E. Thomson, C. D. Campbell, C. Concellón, N. Duguet, K. Rix, A. M. Z. Slawin and A. D. Smith, *J. Org. Chem.*, 2008, **73**, 2784.
- 108 H. Quast and S. Hünig, *Chem. Ber.*, 1966, **99**, 2017.
- 109 A. J. Arduengo, H. V. R. Dias, R. L. Harlow and M. Kline, *J. Am. Chem. Soc.*, 1992, **114**, 5530.

